

Nanoscale

Accepted Manuscript



This is an *Accepted Manuscript*, which has been through the Royal Society of Chemistry peer review process and has been accepted for publication.

Accepted Manuscripts are published online shortly after acceptance, before technical editing, formatting and proof reading. Using this free service, authors can make their results available to the community, in citable form, before we publish the edited article. We will replace this *Accepted Manuscript* with the edited and formatted *Advance Article* as soon as it is available.

You can find more information about *Accepted Manuscripts* in the [Information for Authors](#).

Please note that technical editing may introduce minor changes to the text and/or graphics, which may alter content. The journal's standard [Terms & Conditions](#) and the [Ethical guidelines](#) still apply. In no event shall the Royal Society of Chemistry be held responsible for any errors or omissions in this *Accepted Manuscript* or any consequences arising from the use of any information it contains.

ARTICLE

Selective killing of hepatocellular carcinoma HepG2 cells by three-dimensional nanographene nanoparticles based on triptycene

Cite this: DOI: 10.1039/x0xx00000x

Received 00th January 2012,
Accepted 00th January 2012

DOI: 10.1039/x0xx00000x

www.rsc.org/

Xiaoqin Xiong,^a Lu Gan,^{a*} Ying Liu,^a Chun Zhang,^{a*} Tuying Yong,^a Ziyi Wang,^a Huibi Xu^a and Xiangliang Yang^{a*}

Carbon-based materials have been widely used in the biomedical fields including drug delivery and cancer therapies. In this paper, a recently synthesized three-dimensional nanographene (NG) based on triptycene self-assembles into nanoparticles which selectively kill human hepatocellular carcinoma HepG2 cells as compared to human normal liver HL7702 cells. Obvious differences in cellular accumulation, endocytic pathway and intracellular trafficking of NG nanoparticles are observed in HepG2 cells and HL7702 cells. Further studies reveal that NG nanoparticles significantly increase the levels of reactive oxygen species (ROS) in HepG2 cells, but not in HL7702 cells. NG nanoparticles-induced ROS result in apoptosis induction and the decrease in mitochondrial membrane potential in HepG2 cells. Moreover, IKK/nuclear factor- κ B (NF- κ B) signaling is found to be activated by NG nanoparticles-induced ROS and serves to antagonize NG nanoparticles-induced apoptosis in HepG2 cells. Our studies show that the distinct behaviors of cellular uptake and ROS-mediated cytotoxicity are responsible for the selective killing of HepG2 cells. This study provides a foundation for understanding the mechanism on selective induction of apoptosis in cancer cells by NG nanoparticles and designing more effective chemotherapeutic agents.

Introduction

Cancer is a leading cause of death worldwide. The inability of chemotherapeutics to effectively differentiate between cancer cells and normal cells which results in systemic toxicity might be one of the major problems affecting chemotherapy failure.¹ Therefore, the development of new anticancer drugs which better target cancer cells while sparing normal cells is urgently required.² Nanotechnology-based therapeutics have exhibited the great advantages compared with free drugs, including improved retention, efficacy and safety.³⁻⁵ For example, nanosized therapeutic agents passively accumulate at tumor tissues by enhanced permeability and retention (EPR) effect. In addition, nanoparticles can be conjugated with a specific ligand capable of specifically binding receptors that are overexpressed in cancer cells to increase therapeutic efficiency.^{6,7} Recently, some nanoparticles have been reported to selectively induce apoptosis in tumor cells by initiating the accumulation of intracellular reactive oxygen species (ROS)⁸⁻¹¹ or nanoparticles could synergize with ROS-generating drugs for improved cancer therapy by increasing the intracellular ROS.¹²

Carbon-based materials, typically zero-dimensional fullerenes, one-dimensional nanotubes and two-dimensional

graphene are receiving attention due to their unique electronic, thermal, mechanical and optical properties.^{13,14} Among them, graphene represents one of the most promising carbon materials and has been widely used in the biomedical fields including drug delivery, cancer therapies and biosensing.^{15,16} Recently a novel kind of three-dimensional nanographene (NG) based on triptycene (the structure was shown in Fig. 1A) was synthesized by our group.^{17,18} In this molecule, three hexa-perihexabenzocoronenes units (HBCs) were arrayed in the three-dimensional triptycene scaffold with a well-defined spatial separation, which reduced the face-to-face interaction between π -planes and facilitated the solubilization of HBCs in organic solvents. Our previous work showed that pluronic F68-coated three-dimensional NG nanoparticles could be used as a fluorescent agent for in vitro and in vivo fluorescence imaging.¹⁷ However the potential effects of three-dimensional NG nanoparticles on biological systems, including their cellular uptake and intracellular trafficking, cytotoxicity and biocompatibility, the interaction between NG nanoparticles and biological molecules remain to be elucidated.

In the present study, NG nanoparticles were constructed by evaporation-induced self-assembly method and the effects of NG nanoparticles on the cytotoxicity in carcinoma cells

(including human hepatocellular carcinoma HepG2 cells, human ovarian cancer A2780 cells, human cervical cancer HeLa cells and the paclitaxel-resistant A2780 cells) and normal cells (including human normal liver HL7702 cells and human endothelial ECV304 cells) were determined. The potential mechanism of NG nanoparticles-induced toxicity in a cell-specific manner was further explored by examining their uptake and intracellular localization, the induction of ROS and ROS-related signaling pathway in HepG2 cells and HL7702 cells.

Results

Characterization of NG nanoparticles

To achieve water solubilization of NG based on triptycene, NG nanoparticles were constructed by evaporation-induced self-assembly method. The mean hydrodynamic diameter of NG nanoparticles measured by dynamic light scattering was about 168 nm (Fig. 1B) with a polydispersity of 0.019. TEM imaging showed that NG nanoparticles were monodisperse and spherical with a size distribution of 50-80 nm (Fig. 1C). The UV spectrum of NG nanoparticles displayed the maximal absorption peak at 364 nm. Excitation of the nanoparticles in water at 364 nm resulted in a fluorescence emission at 475 nm, 504 nm and 556 nm (Fig. 1D). The intrinsic fluorescence of NG nanoparticles provides a convenient means to observe and quantify their intracellular trafficking.

Selective killing of cancer cells by NG nanoparticles

To determine the potential biological application of NG nanoparticles, the effects of NG nanoparticles on the viability of human hepatocellular carcinoma HepG2 cells and human normal liver HL7702 cells were determined. After 24 h treatment with NG nanoparticles, the morphology of HepG2 cells changed from spindle shapes to shrunken shapes. In contrast, HL7702 cells maintained their polygon shapes (Fig. S1), implying that NG nanoparticles might induce more cytotoxicity in HepG2 cells than in HL7702 cells. Furthermore, the cell viability induced by NG nanoparticles was evaluated by 3-(4,5-dimethyl-2-thiazolyl)-2,5-Diphenyltetrazolium bromide (MTT) assay. As shown in Fig. 2A, NG nanoparticles induced cytotoxicity in a dose- and time-dependent manner. Exposure to 10 $\mu\text{g/ml}$ NG nanoparticles for 24 h and 48 h strongly inhibited the cell viability of HepG2 cells, reducing cell survival to around 26% and 6%, respectively. However 75% of HL7702 cells still survived even after treatment with 10 $\mu\text{g/ml}$ NG nanoparticles for 48 h. NG nanoparticles at these doses also showed a strong ability to kill other human cancer cells (including ovarian cancer A2780 cells, the paclitaxel-resistant A2780/T cells and cervical cancer HeLa cells) but not human endothelial ECV304 cells (Fig. S2). These results suggested that NG nanoparticles might have a cancer cell-selective killing property.

The percentages of cell apoptosis induced by NG nanoparticles were further investigated in HepG2 cells and HL7702 cells by flow cytometric analysis using Annexin V/PI staining. As shown in Fig. 2B, NG nanoparticles induced cell

apoptosis in a dose-dependent manner. The apoptotic rate of HepG2 cells induced by NG nanoparticles was much more than that of HL7702 cells, which was further confirmed by a more significant increase in PARP cleavage (an apoptotic marker) in HepG2 cells treated with NG nanoparticles (Fig. 2C).

Clonogenic assay was performed to assess the long-term cytotoxicity of NG nanoparticles in HepG2 cells and HL7702 cells. As shown in Fig. 2D, the colony forming capacity of HepG2 cells was significantly inhibited by NG nanoparticles compared with that of HL7702 cells. NG nanoparticles almost completely inhibited the colony forming in HepG2 cells even at the concentration of 0.25 $\mu\text{g/ml}$, however 67% of colonies were survived after treatment with NG nanoparticles at this concentration in HL7702 cells.

Intracellular concentration of NG nanoparticles in HepG2 cells and HL7702 cells

To investigate the possible mechanism of the differential sensitivity to NG nanoparticles between cancer cells and normal cells, HepG2 cells and HL7702 cells were used. Firstly, the intracellular concentration of NG nanoparticles was determined by confocal microscope and fluorescence spectrophotometer. As shown in Fig. 3A, the cellular accumulation of NG nanoparticles increased in a time-dependent manner. However the cellular accumulation of NG nanoparticles in HepG2 cells was significantly higher than that in HL7702 cells. The qualitative results from confocal microscopy studies were further confirmed by the quantitative results obtained from fluorescence spectrophotometer (Fig. 3B), suggesting that the differences in cytotoxicity against HepG2 cells and HL7702 cells might be dependent on the amount of NG nanoparticles internalized.

Cellular uptake and intracellular trafficking of NG nanoparticles in HepG2 cells and HL7702 cells

To elucidate the efficacy of nanoparticle delivery to cells, it is necessary to understand the mechanisms by which nanoparticles are internalized by cells, which will likely determine their ultimate intracellular localization. Therefore, the cellular uptake pathway of NG nanoparticles in HepG2 cells and HL7702 cells were investigated by using several specific endocytic inhibitors.¹⁹ As shown in Fig. 4A, ATP synthesis inhibitors sodium azide (NaN_3)/2-deoxyglucose (DOG) resulted in a marked decrease in the cellular internalization of NG nanoparticles, indicating that the internalization of NG nanoparticles in HepG2 cells and HL7702 cells was an energy-dependent endocytosis. Furthermore, chlorpromazine, an inhibitor to probe clathrin-mediated endocytosis significantly decreased the internalization of NG nanoparticles in HepG2 cells and HL7702 cells. Cytochalasin D, a potent inhibitor of actin polymerization and dynasore, a small cell-permeable molecule which inhibits dynamin GTPase to inhibit both caveolin- and clathrin-mediated pathways as well as macropinocytosis also significantly reduced the cellular uptake of NG nanoparticles in HepG2 cells and HL7702 cells. However the effects of methyl- β -cyclodextrin (M β CD), a cholesterol-depleting agent to disrupt several lipid raft/caveolae-mediated endocytic pathways on the cellular uptake of NG nanoparticles in HepG2 cells were different from that in HL7702 cells. M β CD significantly inhibited the cellular uptake of NG

nanoparticles in HL7702 cells, while no inhibition in cellular uptake of NG nanoparticles was found in HepG2 cells pretreated with M β CD. The qualitative results from confocal microscopy studies were consistent with the quantitative results obtained from fluorescence spectrophotometer (Fig. 4B). These data indicated that both clathrin- and lipid raft/caveolae-mediated endocytic pathways were involved in the internalization of NG nanoparticles in HL7702 cells, whereas clathrin-mediated endocytosis played a predominant role in the uptake of NG nanoparticles in HepG2 cells.

To further determine the intracellular trafficking of NG nanoparticles in HepG2 cells and HL7702 cells after internalization, specific fluorescent dyes and plasmids for expression of green fluorescent protein targeted to organelles were used: 4',6-diamidino-2-phenylindole (DAPI) to label nuclei, LysoTracker Red to label lysosomes, Mito-RFP as a marker for mitochondria and Golgi-RFP as a marker for Golgi complex.²⁰ As shown in Fig. 5, NG nanoparticles were not detected in nucleus in HepG2 and HL7702 cells. NG nanoparticles in HepG2 cells were majorly entrapped in the lysosomes or Golgi apparatus and partially colocalized with mitochondria. However NG nanoparticles almost completely colocalized with lysosomes and largely colocalized with Golgi apparatus in HL7702 cells.

Role of ROS in NG nanoparticles-induced cytotoxicity in HepG2 cells and HL7702 cells

It has been suggested that oxidant generation is the common pathway through which anticancer drugs trigger apoptosis in cancer cells.²¹ To further explore the mechanisms on the selective killing of cancer cells by NG nanoparticles, the effects of NG nanoparticles on intracellular ROS levels in HepG2 cells and HL7702 cells were determined through flow cytometry using the redox-sensitive fluorescent probe 2',7'-dichlorodihydrofluorescein diacetate (H₂DCF-DA). As shown in Fig. 6A, treatment with NG nanoparticles for 3 h caused a marked increase in ROS levels in a dose-dependent manner in HepG2 cells, however very slight increase in ROS levels was induced by NG nanoparticles in HL7702 cells, suggesting that ROS might be involved in NG nanoparticles-induced cell death in HepG2 cells. To further confirm the role of ROS in NG nanoparticles-induced cytotoxicity in HepG2 cells, the effects of N-acetyl-cysteine (NAC), a powerful antioxidant and free radical scavenger on the NG nanoparticles-induced ROS generation and cytotoxicity were examined. As shown in Fig. 6B and C, co-treatment with NAC fully reversed the NG nanoparticles-induced increase in ROS and apoptosis in HepG2 cells. These data suggested that ROS played an important role in NG nanoparticles-induced cytotoxicity in HepG2 cells.

Disruptions of the mitochondrial membrane may cause electron leakage from the mitochondrial respiratory chain, resulting in the formation of ROS and the depolarization of mitochondria.²² Therefore, the mitochondrial membrane potential of HepG2 cells treated with NG nanoparticles was determined by flow cytometry using JC-1 dye. JC-1 accumulates as aggregates in the mitochondria which stains red in healthy cells, whereas JC-1 exists in monomeric form and stains the cytosol green in apoptotic and necrotic cells.²³ As shown in Fig. 6D, HepG2 cells treated with 10 μ g/ml NG

nanoparticles for 3 h exhibited a significant increase in the percentages of JC-1 monomers, however co-treatment with 5 mM NAC abolished the increase in the percentages of JC-1 monomers caused by NG nanoparticles. The data suggested that NG nanoparticles-induced ROS generation was directly associated with the mitochondria dysfunction in HepG2 cells.

Role of IKK/NF- κ B signaling in NG nanoparticles-induced cytotoxicity in HepG2 cells

ROS have been implicated as intracellular signaling molecules in cellular processes such as proliferation, apoptosis and senescence.^{24,25} As it has been shown that ROS-mediated cell cytotoxicity triggers activation of NF- κ B,²⁶ we examined the status of NF- κ B after NG nanoparticles treatment in HepG2 cells. As shown in Fig. 7A, NF- κ B transcriptional activity was significantly enhanced in a dose-dependent manner in HepG2 cells treated with NG nanoparticles using a NF- κ B luciferase reporter gene assay. Co-treatment with NAC markedly reversed the NG nanoparticles-induced NF- κ B activation (Fig. 7B), suggesting that NG nanoparticles-induced ROS was involved in NF- κ B activation in HepG2 cells. To further investigate the mechanism of NF- κ B activation by NG nanoparticles, HepG2 cells were transiently transfected with wild type (WT) or dominant negative forms of IKK α or IKK β protein (IKK α K44A or IKK β -K44A) and then treated with NG nanoparticles. As seen in Fig. 7C and D, IKK α -WT or IKK β -WT significantly increased NG nanoparticles-induced NF- κ B activation, however IKK α K44A or IKK β K44A significantly decreased NG nanoparticles-induced NF- κ B activation, indicating that NG nanoparticles-induced NF- κ B activation might be regulated by IKK α or IKK β . To confirm the role of IKK/NF- κ B signaling in NG nanoparticles-induced cytotoxicity in HepG2 cells, the effects of knocking down NF- κ B activity on NG nanoparticles-induced cytotoxicity was determined. Parthenolide (PN), a natural inhibitor of NF- κ B by preventing I κ B degradation,²⁷ significantly decreased NG nanoparticles-induced cytotoxicity (Fig. 7E). Furthermore, overexpression of IKK α K44A or IKK β K44A significantly enhanced the sensitivity of HepG2 cells to NG nanoparticles (Fig. 7F). These data suggested that IKK/NF- κ B signaling played an important role in NG nanoparticles-induced cytotoxicity and served to antagonize NG nanoparticles-induced apoptosis in HepG2 cells.

Discussion

The understanding of cellular uptake and intracellular trafficking is necessary for clarifying the biological activity of nanomaterials. Besides the size, shape and surface characteristics affect the cellular uptake of nanoparticles, cell type and the nature of cell membrane such as membrane fluidity can influence the uptake pathway of nanoparticle.²⁸ In this paper, nanoparticles were constructed from a recently synthesized three-dimensional nanographene based on triptycene and found to selectively kill HepG2 cells against HL7702 cells. Further studies revealed that both clathrin- and lipid raft/caveolae-mediated endocytic pathways were involved in the internalization of NG nanoparticles in HL7702 cells, whereas the most prominent endocytic pathway of NG nanoparticles in HepG2 cells was clathrin-mediated endocytosis. The different endocytic

pathway in HepG2 cells and HL7702 cells might result in the different amount of NG nanoparticles internalized, which determined the difference in cytotoxicity in HepG2 cells and HL7702 cells. Following cellular uptake of nanoparticles, the subcellular location of nanoparticles also affects the therapeutic function of nanoparticles as well as cytotoxicity. Our work demonstrated that NG nanoparticles translocated to lysosomes and Golgi apparatus in HepG2 cells and HL7702 cells, however some NG nanoparticles might escape from lysosome and localized in mitochondrial in HepG2 cells.

Oxidative stress has been demonstrated to be involved in various physiological and pathological processes, such as cancer. Cancer cells are usually under oxidative stress and, hence, have a relatively high basal level of ROS.²⁹⁻³¹ Several anticancer drugs resulted in a burst of ROS over the threshold of life and death to induce cell death, which was the potential mechanism of action of the anticancer drugs.³² On the other hand, normal cells can better tolerate the oxidative stress because of their lower basal level of ROS and stronger antioxidant capacities.²⁹⁻³¹ Therefore, several compounds such as phenethyl isothiocyanate (PEITC), buthionine sulphoximine (BSO) and piperlongumine have been found to selectively kill cancer cells by inducing ROS without causing significant toxicity to normal cells.^{33,34} In this study, we found that HepG2 cells had much higher basal ROS level compared with HL7702 cells (Fig. 5A). In the meanwhile, NG nanoparticles induced a significant increase in ROS levels in HepG2 cells but not in HL7702 cells. Furthermore, NAC inhibited NG nanoparticles-induced ROS, apoptosis and decreased mitochondrial membrane potential in HepG2 cells. Considering that NG nanoparticles were partially located in mitochondrial in HepG2 cells, NG nanoparticles might impair mitochondrial membrane, release ROS from mitochondrial and even induce apoptosis in HepG2 cells, which might be the main mechanism of selectively killing of HepG2 cells against HL7702 cells.

The cell growth and cell death could be linked to an intracellular ROS level which might be fluctuated in response to intracellular as well as extracellular signals. However, the upregulation of antioxidants and activation of redox-sensitive transcription factors mediating survival signals were usually induced to counteract oxidative stress as an adaptation response in cancer chemotherapy.^{35,36} The balance between these two antagonizing signals ultimately determined when and whether the stimulated cells would die. NF- κ B, a redox-sensitive transcription factor, plays a major role in various cellular processes including inflammation, cell survival, apoptosis, invasion and angiogenesis.³⁷ In most unstimulated cells, NF- κ B dimers are retained in an inactive form in the cytosol through their interaction with the inhibitor of NF- κ B (I κ B) proteins. In response to a variety of stimuli, I κ B kinase (IKK) complex consisting of two catalytic subunits (IKK α and IKK β) and a regulatory subunit (IKK γ) can phosphorylate the I κ B proteins, resulting in nuclear translocation of NF- κ B and transcription activation of its target genes.³⁷ Recent studies have yielded conflicting results about the effect of NF- κ B on apoptosis.³⁸ NF- κ B was reported to not only activate the apoptotic machinery but also enhance cellular defenses and promote cell survival depending on the levels of the p65 and cRel subunits. In this paper, we found that

NF- κ B transcriptional activity was upregulated by NG nanoparticles-induced ROS in HepG2 cells and IKK α /IKK β played an important role in the regulation of NG nanoparticles-induced NF- κ B activation. Furthermore we provided evidence that NF- κ B signaling served to antagonize NG nanoparticles-induced apoptosis in HepG2 cells considering that NF- κ B inhibitor or dominant-negative forms of IKK inhibited NG nanoparticles-induced apoptosis in HepG2 cells. Our findings indicated that NG nanoparticles resulted in elevated ROS production to attack cancer cells, which activated NF- κ B to antagonize ROS-induced cytotoxicity. Therefore, codelivery of NF- κ B inhibitor and NG nanoparticles might be needed to achieve the better anticancer efficiency of NG nanoparticles.

Our work showed that distinct behaviors of cellular uptake and ROS-mediated cytotoxicity might be responsible for the selective killing of cancer cells (Fig. 8). The inherent differential toxicity of NG nanoparticles on cancer cells raises opportunities for their potential use as anticancer agents. Considering that nanoparticles were usually passively accumulated at tumor tissues by EPR effect, the antitumor activity and the biodistribution of NG nanoparticles *in vivo* need to be further explored. Furthermore, the selectivity and the antitumor activity of NG nanoparticles might be enhanced by conjugating tumor targeting ligands such as monoclonal antibodies, peptides and small molecules to tumor-associated proteins. With the intrinsic fluorescence, NG nanoparticles might have the potential to be used as a multifunctional theranostic platform in cancer treatment.

Experimental Section

Materials

MTT, H₂DCF-DA, chlorpromazine, NaN₃, DOG, dynasore, cytochalasin D, M β CD and complete protease inhibitor cocktail were purchased from Sigma-Aldrich (St Louis, MO, USA). LysoTracker Red, DAPI and NAC were purchased from Beyotime Institute of Biotechnology (Shanghai, China). Parthenolide was purchased from Qebio Science & Technologies Co., Ltd (Shanghai, China). All other chemicals used were of analytical grade commercially available.

Plasmid amplification

Plasmids for FLAG-IKK α , FLAG-IKK β , FLAG-IKK α K44A and FLAG-IKK β K44A were kindly provided by Prof. Hongbing Shu (Wuhan University, Wuhan, China). Plasmids expressing Mito-RFP and Golgi-RFP were kindly provided by Prof. Jingyu Liu (Huazhong University of Science and Technology, Wuhan, China). Plasmids for 3 \times κ B-Luc firefly and *Renilla* luciferase reporter genes were kindly provided by Dr. Shuai Chen (Institute of Microbiology, Chinese Academy of Sciences, Beijing, China). To amplify these plasmids, plasmids were proliferated firstly in *Escherichia coli* DH5a strain and then purified using QIAGEN plasmid purification kits (QIAGEN Sciences Inc, Germantown, MD, USA) following the manufacturer's instructions. The plasmids obtained were identified by sequencing. The concentration and purity of plasmid preparations were determined by UV spectrophotometry.

Cell culture

The human hepatocellular carcinoma cell line HepG2, human normal liver cell line HL7702 and human cervical carcinoma cell line HeLa were purchased from Type Culture Collection of the Chinese Academy of Sciences (Shanghai, China). The human ovarian carcinoma cell line A2780 was kindly provided by Dr. Ding Ma (Huazhong University of Science and Technology, Wuhan, China). The paclitaxel-resistant A2780 cell line (A2780/T) was purchased from KeyGen Biotech Co. Ltd (Nanjing, China). The cells were cultured in DMEM medium except that A2780/T cells were cultured in DMEM medium containing 800 ng/ml paclitaxel at 37 °C in 5% CO₂ in a humidified atmosphere. All medium contained 10% FBS (Gibco BRL/Life Technologies, Grand Island, NY, USA), 100 U/ml penicillin and 100 µg/ml streptomycin.

Preparation and characterization of NG nanoparticles

The three-dimensional NG based on triptycene was synthesized as described.¹⁵ The NG nanoparticles were fabricated by evaporation-induced self-assembly method.³⁹ Briefly, 1 mg NG was pre-dissolved in 1 ml tetrahydrofuran (THF) and added dropwise to 10 ml water under magnetic stirring. THF in the solution was then removed by rotary evaporation under reduced pressure at 40 °C. The hydrodynamic size of NG nanoparticles was determined by dynamic light scattering (DLS; ZetaSizer ZS90, Malvern Instruments, Malvern, UK). The morphology of NG nanoparticles was observed via transmission electron microscopy (TEM; Tecnai G2 20, FEI Corporation, Eindhoven, Netherlands).

Gene transfection

Transfections by electroporation were performed as described.⁴⁰ Briefly, the cells were trypsinized and 1×10^6 cells were resuspended in 350 µl Opti-MEM medium. 10 µg plasmid DNA was diluted in 50 µl Opti-MEM medium and then added into the resuspended cells. The mixtures of cells and DNA were kept at room temperature for 5 min and then transferred into a 4-mm cuvette. The electroporation was carried out using Gene Pulser II Electroporation System (Bio-Rad, Richmond, CA, USA). The electroporated cells were replated into 3 wells in the 6-well plates and cultured with DMEM medium containing 10% FBS for 24 h. Approximately 75-90% transfection efficiencies were routinely achieved.

Cell cytotoxicity assay

Cell cytotoxicity was determined using a standard MTT assay.⁴¹ Briefly, cells were plated in 96-well plates at a density of 1×10^3 cells/well. The cells were treated with different concentrations of NG nanoparticles. At the indicated time points, the cells were washed with PBS and then 20 µl of 5 mg/ml MTT solution was added to the cells in each well. Plates were incubated for an additional 2 h at 37 °C. The medium containing MTT was removed and 150 µl DMSO was added to dissolve the formazan crystals formed by living cells.

Absorbance was measured at 490 nm using a Labsystems iEMS microplate reader (Helsinki, Finland).

Apoptotic cell death assay

Cells were grown in 6-well plates and treated with different concentrations of NG nanoparticles. After 24 h treatment, the cells were collected and washed with PBS. Apoptosis was measured using an Annexin V/PI apoptosis detection kit according to the manufacturer's instructions (MultiSciences Biotech Co. Ltd, Hangzhou, China) and analyzed by a Cytomics™ FC 500 flow cytometer (Beckman Coulter, Fullerton, CA, USA). A quadrant analysis was performed and cells stained positive for Annexin V-FITC and/or PI were designated as apoptotic and unstained cells were designated as alive.

Colony forming assay

Cells were trypsinized to make a single cell suspension and plated in 6-well plates at a density of 1×10^3 cells/well. The cells were incubated in the medium containing different concentrations of NG nanoparticles and then changed the medium every three days. After 10 days incubation, the cells were fixed with 4% paraformaldehyde followed by staining using 1% crystal violet. The plates were photographed and colonies containing at least 100 cells were counted.

Cellular accumulation of NG nanoparticles

Cells were grown in 6-well plates and incubated in serum-free DMEM medium containing 10 µg/ml NG nanoparticles. After treatment for different time courses, the cells were washed with PBS and examined under an Andor Revolution spinning disk confocal microscope (Andor Technology, Germany). Images were recorded using standard filter sets (excitation at 491 nm and emission at 495-550 nm). For quantitative analysis, the cells were harvested and lysed with 100 µl PBS containing 1% Triton X-100. Cell lysates were mixed with 400 µl THF and then centrifuged at 12,000 rpm for 5 min. The fluorescence intensity of the supernatants was analyzed by F-4500 fluorescence spectrophotometer (Hitachi Ltd., Tokyo, Japan) with the excitation wavelength at 363 nm and emission wavelength at 473 nm. The cellular accumulation of NG nanoparticles was defined as normalization of fluorescence intensity of NG with respect to total protein content. The protein contents were determined using the BCA protein assay kit (Beyotime Institute of Biotechnology, Shanghai, China) according to the manufacturer's instructions.

Endocytic pathway of NG nanoparticles

To study the endocytic pathway involved in the internalization of NG nanoparticles, the cells were preincubated in serum-free DMEM medium with 0.1% NaN₃/DOG (1 h), 5 mM MβCD (15 min), 10 µg/ml chlorpromazine (15 min), 80 µM dynasore (30 min) or 10 µg/ml cytochalasin D (1 h), respectively. The medium was then changed to fresh serum-free medium containing the inhibitors plus 10 µg/ml NG nanoparticles and further incubated for 1 h at 37 °C. The cells were washed with

PBS and imaged by Andor Revolution spinning disk confocal microscope. For quantitative analysis of the intracellular concentration of NG nanoparticles after treatment with the inhibitors, the cells were harvested, lysed and the fluorescence intensity of the supernatants was determined by F-4500 fluorescence spectrophotometer.

Intracellular localization of NG nanoparticles

For assessment of colocalization of NG nanoparticles with mitochondrial or Golgi apparatus, the cells were transfected with Mito-RFP (mitochondrial marker) or Golgi-RFP (Golgi marker), respectively. After 24 h transfection, the cells were treated with 10 $\mu\text{g/ml}$ NG nanoparticles for 3 h, washed with PBS and then fixed in 4% paraformaldehyde for 15 min at room temperature. For assessment of colocalization of NG nanoparticles with lysosome or nucleus, the cells were treated with 10 $\mu\text{g/ml}$ NG nanoparticles for 3 h, washed with PBS and then incubated with medium containing 100 nM LysoTracker Red (a lysosomal marker) at 37 $^{\circ}\text{C}$ for 30 min before fixation or stained with 5 $\mu\text{g/ml}$ DAPI (labeling cell nuclei) after fixation, respectively. The cells were observed under an Andor Revolution spinning disk confocal microscope.

Measurement of intracellular ROS

Intracellular ROS levels were measured using the oxidant-sensitive fluorogenic probe $\text{H}_2\text{DCF-DA}$.⁴² Briefly, after treatment with different concentrations of NG nanoparticles for 3 h, the cells were harvested and incubated with 5 μM $\text{H}_2\text{DCF-DA}$ in PBS at 37 $^{\circ}\text{C}$ for 30 min. The cells were washed with PBS twice to remove the extracellular $\text{H}_2\text{DCF-DA}$ and the intracellular ROS was analyzed using a CytomicsTM FC 500 flow cytometer.

Mitochondrial membrane potential assay

Mitochondrial membrane potential was determined using mitochondrial membrane potential assay kit with JC-1 probe (Beyotime Institute of Biotechnology, Shanghai, China). Briefly, after treatment with 10 $\mu\text{g/ml}$ NG nanoparticles in the presence or absence of 5 mM NAC for 3 h, the cells were collected and stained with 5 $\mu\text{g/ml}$ JC-1 solution at 37 $^{\circ}\text{C}$ for 20 min. The cells were washed with PBS twice and resuspended in 500 μl fresh cell culture medium. Cells were analyzed using a CytomicsTM FC 500 flow cytometer.

NF- κB luciferase activity assay

The cells were transfected with the indicated plasmids in combination with plasmids for $3\times\kappa\text{B-Luc}$ firefly and Renilla luciferase reporter genes. After 36 h transfection, the cells were treated with 10 $\mu\text{g/ml}$ NG nanoparticles for 6 h. The cells were harvested and firefly and *Renilla* luciferase activities in cell lysates were measured using the Dual-Luciferase reporter assay system (Promega, Madison, WI, USA). Renilla luciferase activities of cells were used as internal control.

Western blot analysis

The cells were treated with different concentrations of NG nanoparticles. After 24 h treatment, the cells were harvested and subjected to western blot. Briefly, the cells were lysed in the ice cold lysis buffer containing 62.5 mM Tris-HCl (pH 6.8), 2 mM EGTA, 2% SDS, 10% glycerol, 10 mM NaF, 0.1% Triton X-100, 2 mM Na_3VO_4 and complete protease inhibitor cocktail. The cell lysates (40 μg) were separated by 10% SDS-PAGE and transferred onto a PVDF membrane. The membrane was blocked with 5% skin milk in TBS containing 0.1% Tween 20 (TBST) for 1 h and then probed with the indicated primary antibody overnight at 4 $^{\circ}\text{C}$, respectively. The membrane was washed with TBST $3\times$ for 5 min. After incubation with horseradish peroxidase (HRP)-conjugated secondary antibody, protein signals were detected using enhanced chemiluminescence (Perice, Rockford, IL, USA). The primary antibodies used were anti-PARP (Cell Signaling Technology, Danvers, MA, USA); anti-FLAG (M2) (Sigma-Aldrich, St Louis, MO, USA); anti- β -actin (Santa Cruz Biotechnology, Santa Cruz, CA, USA).

Statistical Analysis

Experiments were carried out with three or four replicates. Statistical analyses were performed by Student's t test. Values with $P < 0.05$ are considered significant.

Conclusions

In this study, the cytotoxicity of NG nanoparticles against cancer cells and its potential mechanisms were determined. The results showed that obvious differences in intracellular accumulation, cellular uptake and intracellular trafficking might result in selective cytotoxicity of NG nanoparticles against human hepatocellular carcinoma HepG2 cells compared with human normal liver HL7702 cells. Furthermore, ROS played an important role in NG nanoparticles-induced cytotoxicity in HepG2 cells and IKK/NF- κB signaling were involved in NG nanoparticles-induced cytotoxicity. These findings provide guidance for the design of more effective chemotherapeutic agents.

Acknowledgements

We thank Prof. Ding Ma for the cells and Profs. Hongbing Shu, Jingyu Liu and Shuai Chen for the plasmids. We also thank the Analytical and Testing Center of Huazhong University of Science and Technology for related analysis. This work was supported by National Basic Research Program of China (973 Programs, 2012CB932500, 2011CB933100 and 2015CB931800), the National Natural Science Foundation of China (31070689, 81372400 and 20902031), the Natural Science Foundation of Hubei Province (2013CFB163) and the Fundamental Research Funds for the Center Universities (HUST: 2012TS013).

References

- 1 V. Guillemard and H. U. Saragovi, *Curr. Cancer Drug Targets*, 2004, **4**, 313–326.
- 2 R. V. Chari, *Acc. Chem. Res.*, 2008, **41**, 98–107.
- 3 M. Wang and M. Thanou, *Pharmacol. Res.*, 2010, **62**, 90–99.
- 4 M. Rahman, M. Z. Ahmad, I. Kazmi, S. Akhter, M. Afzal, G. Gupta and V. R. Sinha, *Curr. Drug Discov. Technol.*, 2012, **9**, 319–329.
- 5 J. Drbohlavova, J. Chomoucka, V. Adam, M. Ryvolova, T. Eckschlager, J. Hubalek and R. Kizek, *Curr. Drug Metab.*, 2013, **14**, 547–564.
- 6 F. Danhier, O. Feron and V. Préat, *J. Control. Release*, 2010, **148**, 135–146.
- 7 S. Acharya, F. Dilnawaz and S. K. Sahoo, *Biomaterials*, 2009, **30**, 5737–5750.
- 8 M. J. Akhtar, M. Ahamed, S. Kumar, M. M. Khan, J. Ahmad and S. A. Alrokayan, *Int. J. Nanomedicine*, 2012, **7**, 845–857.
- 9 L. Wang, Y. Liu, W. Li, X. Jiang, Y. Ji, X. Wu, L. Xu, Y. Qiu, K. Zhao, T. Wei, Y. Li, Y. Zhao and C. Chen, *Nano Lett.*, 2011, **11**, 772–780.
- 10 T. Xia, M. Kovichich, J. Brant, M. Hotze, J. Sempf, T. Oberley, C. Sioutas, J. I. Yeh, M. R. Wiesner and A. E. Nel, *Nano Lett.*, 2006, **6**, 1794–1807.
- 11 L. Yan, Z. Gu and Y. Zhao, *Chem. Asian J.*, 2013, **8**, 2342–2353.
- 12 G. Huang, H. Chen, Y. Dong, X. Luo, H. Yu, Z. Moore, E. A. Bey, D. A. Boothman and J. Gao, *Theranostics*, 2013, **3**, 116–126.
- 13 J. N. Tiwari, R. N. Tiwari and K. S. Kim, *Prog. Mater. Sci.*, 2012, **57**, 724–803.
- 14 Y. Zhai, Y. Dou, D. Zhao, P. F. Fulvio, R. T. Mayes and S. Dai, *Adv. Mater.*, 2011, **23**, 4828–4850.
- 15 Y. Zhang, D. Petibone, Y. Xu, M. Mahmood, A. Karmakar, D. Casciano, S. Ali and A. S. Biris, *Drug Metab. Rev.*, 2014, **46**, 232–246.
- 16 D. J. Lim, M. Sim, L. Oh, K. Lim and H. Park, *Arch. Pharm. Res.*, 2014, **37**, 43–52.
- 17 C. Zhang, Y. Liu, X. Q. Xiong, L. H. Peng, L. Gan, C. F. Chen and H. B. Xu, *Org. Lett.*, 2012, **14**, 5912–5915.
- 18 P. C. Zhu, L. N. Luo, P. Q. Cen, J. T. Li and C. Zhang, *Tetrahedron Lett.*, 2014, **55**, 6277–6280.
- 19 L. Xiao, X. Xiong, X. Sun, Y. Zhu, H. Yang, H. Chen, L. Gan, H. Xu and X. Yang, *Biomaterials*, 2011, **32**, 5148–5157.
- 20 Z. Zhang, X. Xiong, J. Wan, L. Xiao, L. Gan, Y. Feng, H. Xu and X. Yang, *Biomaterials*, 2012, **33**, 7233–7240.
- 21 G. T. Wondrak, *Antioxid. Redox Signal.*, 2009, **11**, 3013–3069.
- 22 V. Gogvadze, S. Orrenius and B. Zhivotovsky, *Trends Cell Biol.*, 2008, **18**, 165–173.
- 23 S. T. Smiley, M. Reers, C. Mottola-Hartshorn, M. Lin, A. Chen, T. W. Smith, G. D. Jr. Steele and L. B. Chen, *Proc. Natl. Acad. Sci. USA*, 1991, **88**, 3671–3675.
- 24 M. Benhar, D. Engelberg and A. Levitzki, *EMBO Rep.*, 2002, **3**, 420–425.
- 25 M. Benhar, I. Dalyot, D. Engelberg and A. Levitzki, *Mol. Cell Biol.*, 2001, **21**, 6913–6926.
- 26 N. C. Yip, I. S. Fombon, P. Liu, S. Brown, V. Kannappan, A. L. Armesilla, B. Xu, J. Cassidy, J. L. Darling and W. Wang, *Br. J. Cancer*, 2011, **104**, 1564–1574.
- 27 M. Sheehan, H. R. Wong, P. W. Hake, V. Malhotra, M. O'Connor and B. Zingarelli, *Mol. Pharmacol.*, 2002, **61**, 953–963.
- 28 C. Peetla, S. Jin, J. Weimer, A. Elegbede and V. Labhsetwar, *Langmuir*, 2014, **30**, 7522–7532.
- 29 T. P. Szatrowski and C. F. Nathan, *Cancer Res.*, 1991, **51**, 794–798.
- 30 S. Toyokuni, K. Okamoto, J. Yodoi and H. Hiai, *FEBS Lett.*, 1995, **358**, 1–3.
- 31 P. T. Schumacker, *Cancer Cell*, 2006, **10**, 175–176.
- 32 D. Trachootham, J. Alexandre and P. Huang, *Nat. Rev. Drug Discov.*, 2009, **8**, 579–591.
- 33 D. Trachootham, Y. Zhou, H. Zhang, Y. Demizu, Z. Chen, H. Pelicano, P. J. Chiao, G. Achanta, R. B. Arlinghaus, J. Liu and P. Huang, *Cancer Cell*, 2006, **10**, 241–252.
- 34 L. Raj, T. Ide, A. U. Gurkar, M. Foley, M. Schenone, X. Li, N. J. Tolliday, T. R. Golub, S. A. Carr, A. F. Shamji, A. M. Stern, A. Mandinova, S. L. Schreiber and S. W. Lee, *Nature*, 2011, **475**, 231–234.
- 35 M. B. Irmak, G. Ince, M. Ozturk and R. Cetin-Atalay, *Cancer Res.*, 2003, **63**, 6707–6715.
- 36 T. W. Young, F. C. Mei, G. Yang, J. A. Thompson-Lanza, J. Liu and X. Cheng, *Cancer Res.*, 2004, **64**, 4577–4584.
- 37 H. Zheng, Q. Li, R. Chen, J. Zhang, Y. Ran, X. He, S. Li and H. B. Shu, *J. Biol. Chem.*, 2013, **288**, 819–825.
- 38 B. Kaltschmidt, C. Kaltschmidt, T. G. Hofmann, S. P. Hehner, W. Dröge, M. L. Schmitz, *Eur. J. Biochem.*, 2000, **267**, 3828–3835.
- 39 J. P. Hill, W. Jin, A. Kosaka, T. Fukushima, H. Ichihara, T. Shimomura, K. Ito, T. Hashizume, N. Ishii and T. Aida, *Science*, 2004, **304**, 1481–1483.
- 40 L. Gan, P. Liu, H. Lu, S. Chen, J. Yang, J. B. McCarthy, K. E. Knudsen and H. Huang, *Cell Death Differ.*, 2009, **16**, 1408–1417.
- 41 M. Hanelt, M. Gareis and B. Kollarczik, *Mycopathologia* 1994, **128**, 167–174.
- 42 Y. Murata, Z. M. Pei, I. C. Mori and J. Schroeder, *Plant Cell*, 2011, **13**, 2513–2523.

Notes

^a National Engineering Research Center for Nanomedicine, College of Life Science and Technology, Huazhong University of Science and Technology, Wuhan 430074, China. Fax: +86 27 8779 2234; Tel: +86 27 8779 2147; E-mail: lugan@mail.hust.edu.cn, chunzhang@mail.hust.edu.cn, yangxl@mail.hust.edu.cn

Electronic Supplementary Information (ESI) available: [details of any supplementary information available should be included here]. See DOI: 10.1039/b000000x/

Figure Legends

Fig.1 Characterization of three-dimensional NG nanoparticles. (A) The structure of NG based on triptycene. (B) The hydrodynamic size of NG nanoparticles. (C) TEM image of NG nanoparticles. The scale bar is 100 nm (left) and 50 nm (right). (D) The fluorescent spectrum of three-dimensional NG nanoparticles.

Fig. 2 The cytotoxicity of NG nanoparticles in HepG2 cells and HL7702 cells. (A) Cell viabilities of HepG2 cells and HL7702 cells treated with different concentrations of NG nanoparticles for 24 h or 48 h by MTT assay. * $P < 0.01$ compared with HL7702 group at the corresponding concentration. (B) Percentages of apoptosis in HepG2 cells and HL7702 cells treated with different concentrations of NG nanoparticles for 24 h by Annexin V/PI staining. Results from one representative experiment were shown on the left. Quantitative results were shown on the right. (C) PARP cleavage induced by different concentrations of NG nanoparticles in HepG2 cells and HL7702 cells for 24 h by western blotting. β -actin was used as a loading control. (D) The colony forming of HepG2 cells and HL7702 cells treated with different concentrations of NG nanoparticles for 10 days. Results from one representative experiment were shown on the left. Quantitative results were shown on the right. Data as mean values \pm S.D. ($n = 3$). * $P < 0.01$.

Fig.3 The intracellular accumulation of NG nanoparticles in HepG2 cells and HL7702 cells treated with 10 $\mu\text{g/ml}$ NG nanoparticles for different time courses. (A) Confocal microscope images of HepG2 cells and HL7702 cells incubated with 10 $\mu\text{g/ml}$ NG nanoparticles for different time courses. The scale bar is 50 μm . (B) The fluorescence intensity of NG in HepG2 cells and HL7702 cells incubated with 10 $\mu\text{g/ml}$ NG nanoparticles for different time courses by fluorescence spectrophotometer. Data as mean values \pm S.D. ($n = 3$). * $P < 0.01$.

Fig. 4 The endocytic pathway of NG nanoparticles in HepG2 cells and HL7702 cells. (A) Confocal microscope images of HepG2 cells and HL7702 cells preincubated with serum-free medium (control), 0.1% NaN_3/DOG , 10 $\mu\text{g/ml}$ chlorpromazine, 5 mM $\text{M}\beta\text{CD}$, 80 μM dynasore or 10 $\mu\text{g/ml}$ cytochalasin D followed by coincubation with 10 $\mu\text{g/ml}$ NG nanoparticles for 1 h. The scale bar is 50 μm . (B) Internalized fluorescence intensity of NG in HepG2 cells and HL7702 cells treated with the specific endocytic inhibitors as above followed by coincubation with 10 $\mu\text{g/ml}$ NG nanoparticles for 1 h using fluorescence spectrophotometer. Data as mean values \pm S.D. ($n = 3$). * and # $P < 0.01$ compared with the respective control.

Fig. 5 Confocal microscopy images of the intracellular trafficking of NG nanoparticles after HepG2 cells and HL7702 cells transfected with Mito-RFP or Glogi-RFP were treated with 10 $\mu\text{g/ml}$ NG nanoparticles for 3 h, or HepG2 cells and HL7702 cells were treated with 10 $\mu\text{g/ml}$ NG nanoparticles for 3 h and then labeled with 100 nM LysoTracker Red or 5 $\mu\text{g/ml}$ DAPI, respectively. The scale bar is 20 μm .

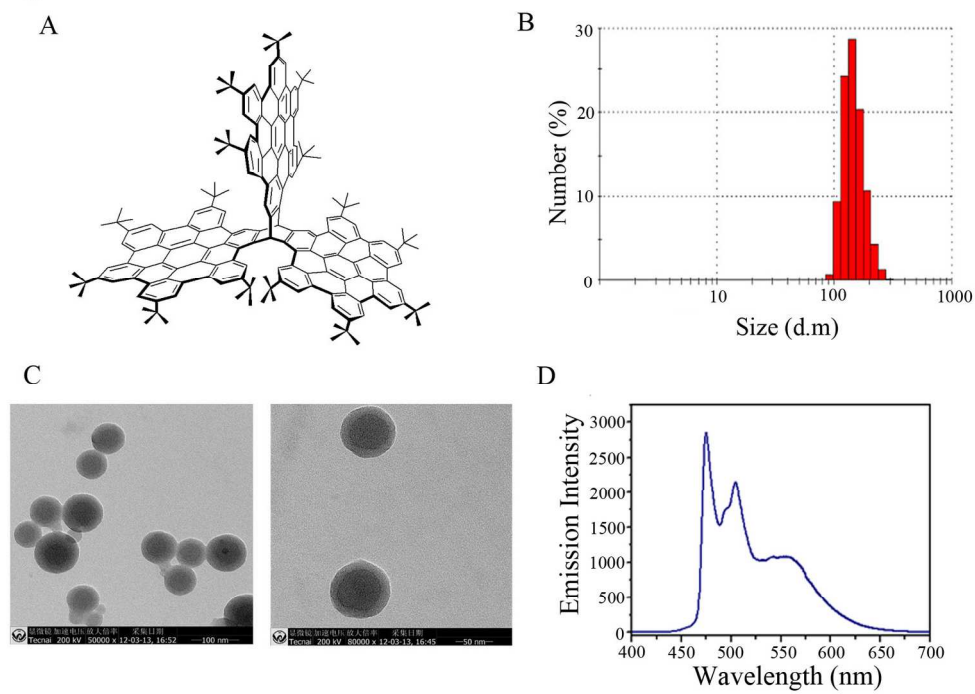
Fig. 6 Effects of ROS on NG nanoparticles-induced cytotoxicity in HepG2 cells. (A) Induction of intracellular ROS in HepG2 cells and HL7702 cells treated with different concentrations of NG nanoparticles for 3 h by $\text{H}_2\text{DCF-DA}$ staining. (B) Changes of

intracellular ROS in HepG2 cells treated with 10 $\mu\text{g/ml}$ NG nanoparticles in the presence or absence of 5 mM NAC for 3 h by $\text{H}_2\text{DCF-DA}$ staining. (C) The percentages of apoptosis in HepG2 cells treated with 10 $\mu\text{g/ml}$ NG nanoparticles in the presence or absence of 5 mM NAC for 24 h by Annexin V/PI staining. Results from one representative experiment were shown on the left. Quantitative results were shown on the right. (D) Mitochondrial membrane potential in HepG2 cells treated with 10 $\mu\text{g/ml}$ NG nanoparticles in the presence or absence of 5 mM NAC for 24 h by JC-1 staining. Results from one representative experiment were shown on the left. Quantitative results were shown on the right. Data as mean values \pm S.D. ($n = 3$). * $P < 0.01$.

Fig. 7 Effects of IKK/NF- κB signaling on NG nanoparticles-induced cytotoxicity in HepG2 cells. (A) NF- κB luciferase activities in HepG2 cells treated with different concentrations of NG nanoparticles for 6 h. (B) NF- κB luciferase activities in HepG2 cells treated with 10 $\mu\text{g/ml}$ NG nanoparticles in the presence or absence of 5 mM NAC for 6 h. (C) NF- κB luciferase activities in FLAG-IKK α -, FLAG-IKK β - or pcDNA 3.1-transfected HepG2 cells after treatment with or without 10 $\mu\text{g/ml}$ NG nanoparticles for 6 h. The protein expression of the transfected plasmids in HepG2 cells was shown below. β -actin was used as a loading control. (D) NF- κB luciferase activities in FLAG-IKK α K44A-, FLAG-IKK β K44A- or pcDNA 3.1-transfected HepG2 cells after treatment with or without 10 $\mu\text{g/ml}$ NG nanoparticles for 6 h. The protein expression of the transfected plasmids in HepG2 cells was shown below. β -actin was used as a loading control. (E) Cell viabilities of HepG2 cells treated with different concentrations of NG nanoparticles in the presence or absence of 5 μM parthenolide for 24 h by MTT assay. Data as mean values \pm S.D. ($n = 3$). * $P < 0.01$ compared with NG nanoparticles-treated group at the corresponding concentration. (F) Cell viabilities of FLAG-IKK α K44A-, FLAG-IKK β K44A- or pcDNA 3.1-transfected HepG2 cells after treatment with different concentrations of NG nanoparticles for 24 h by MTT assay. Data as mean values \pm S.D. ($n = 3$). * $P < 0.05$, ** $P < 0.01$ compared with pcDNA3.1-transfected group at the corresponding concentration.

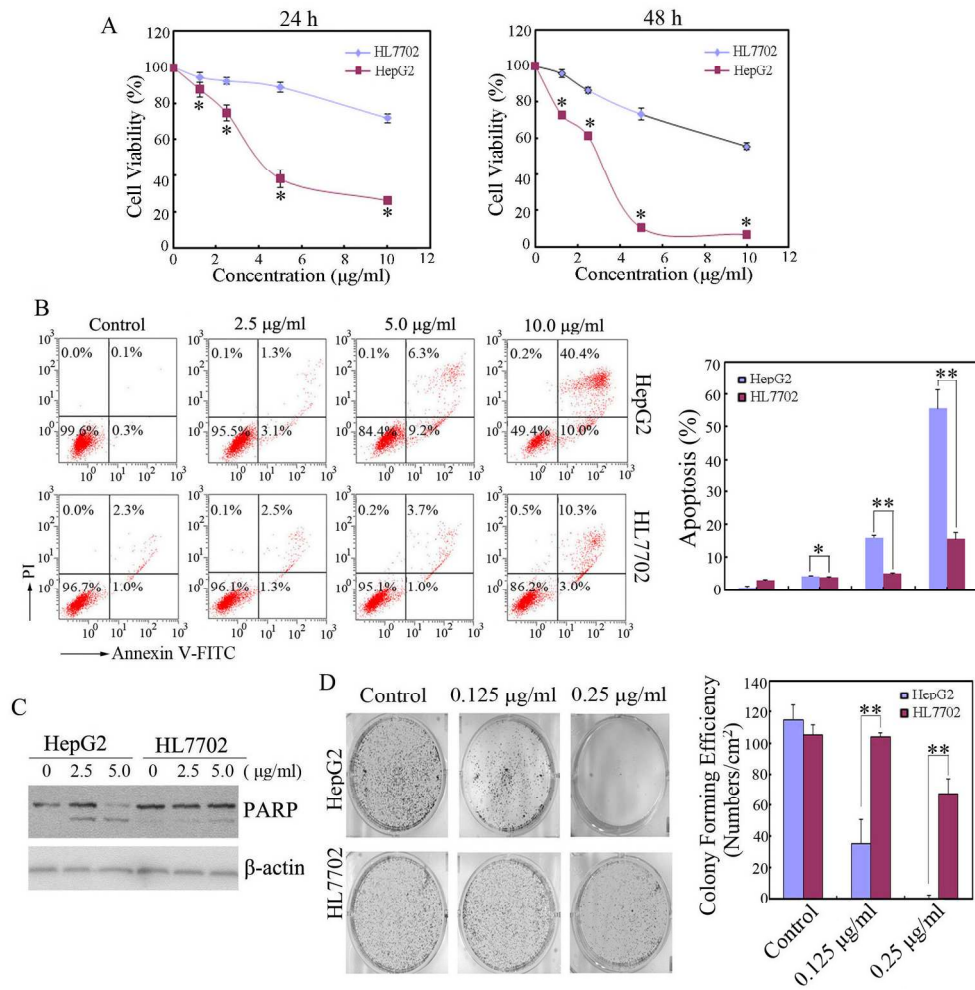
Fig.8 Proposed mechanism for selective killing of HepG2 cells by NG nanoparticles as compared to HL7702 cells.

Figure 1



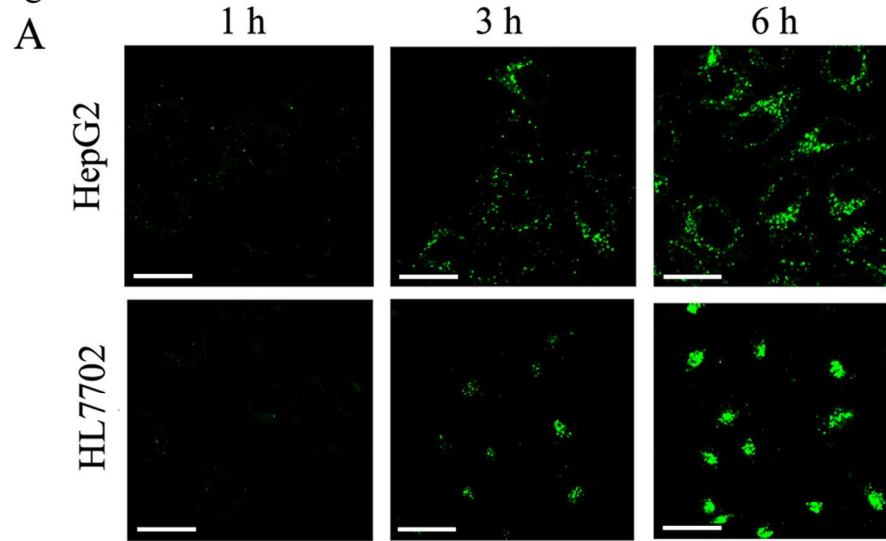
156x116mm (300 x 300 DPI)

Figure 2

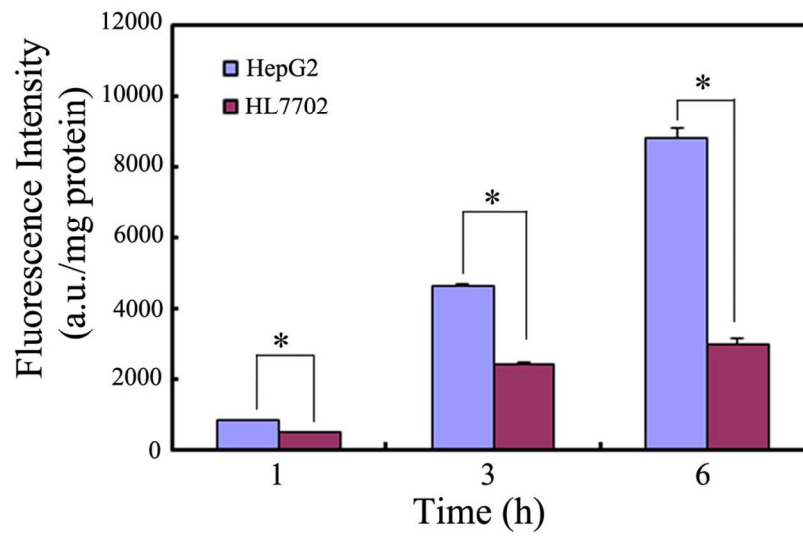


177x185mm (300 x 300 DPI)

Figure 3

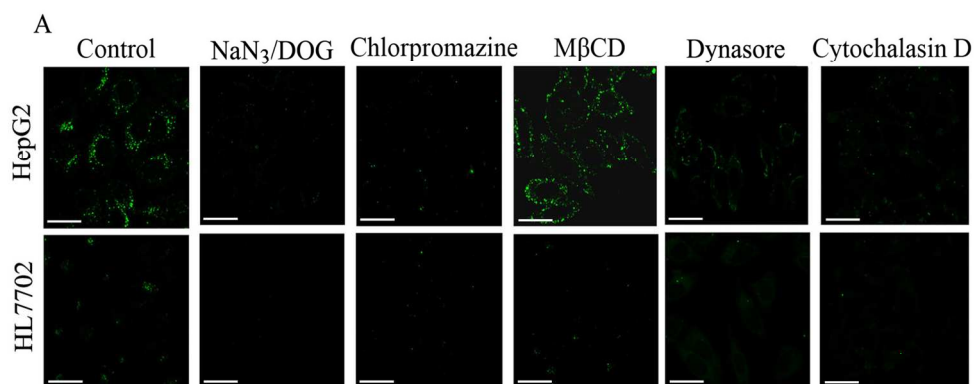


B

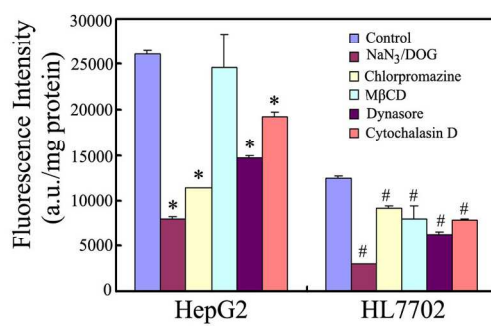


105x134mm (300 x 300 DPI)

Figure 4

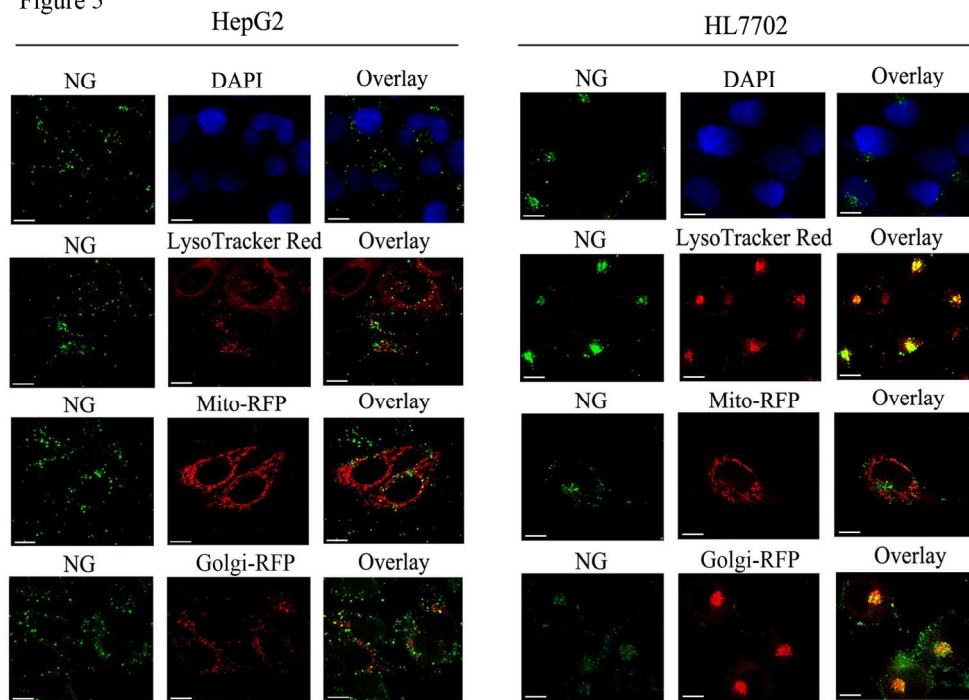


B



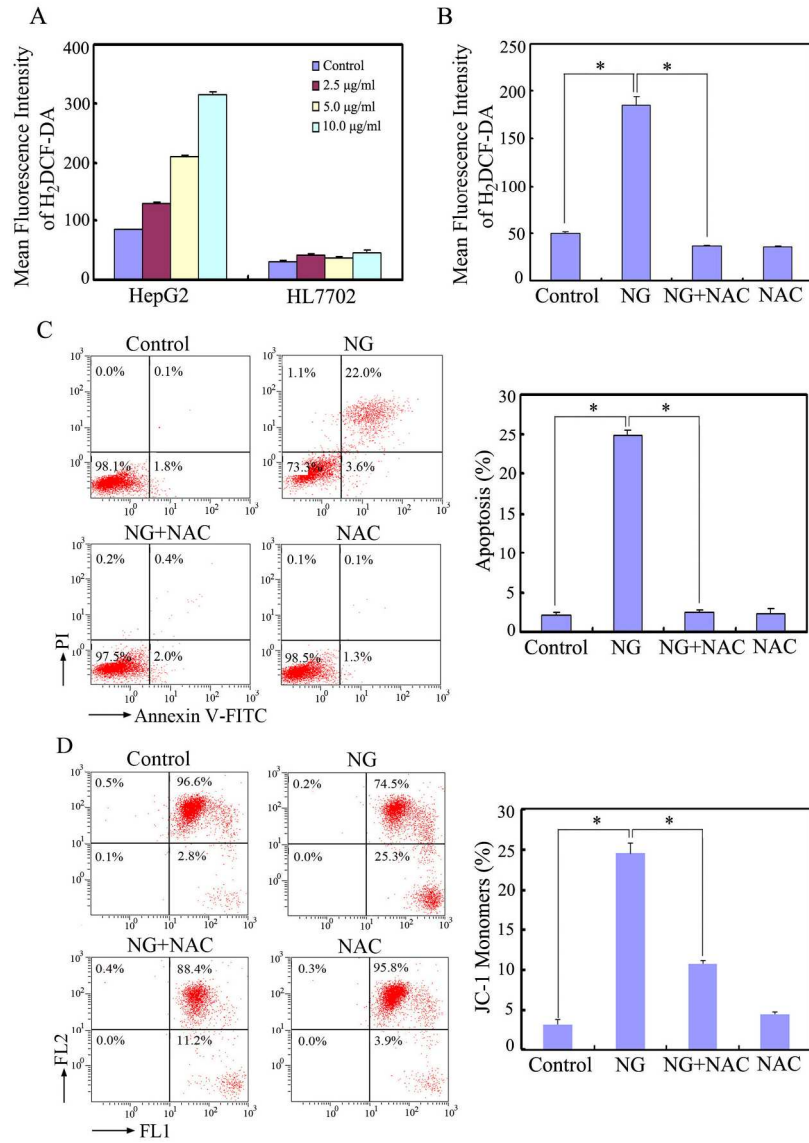
166x129mm (300 x 300 DPI)

Figure 5



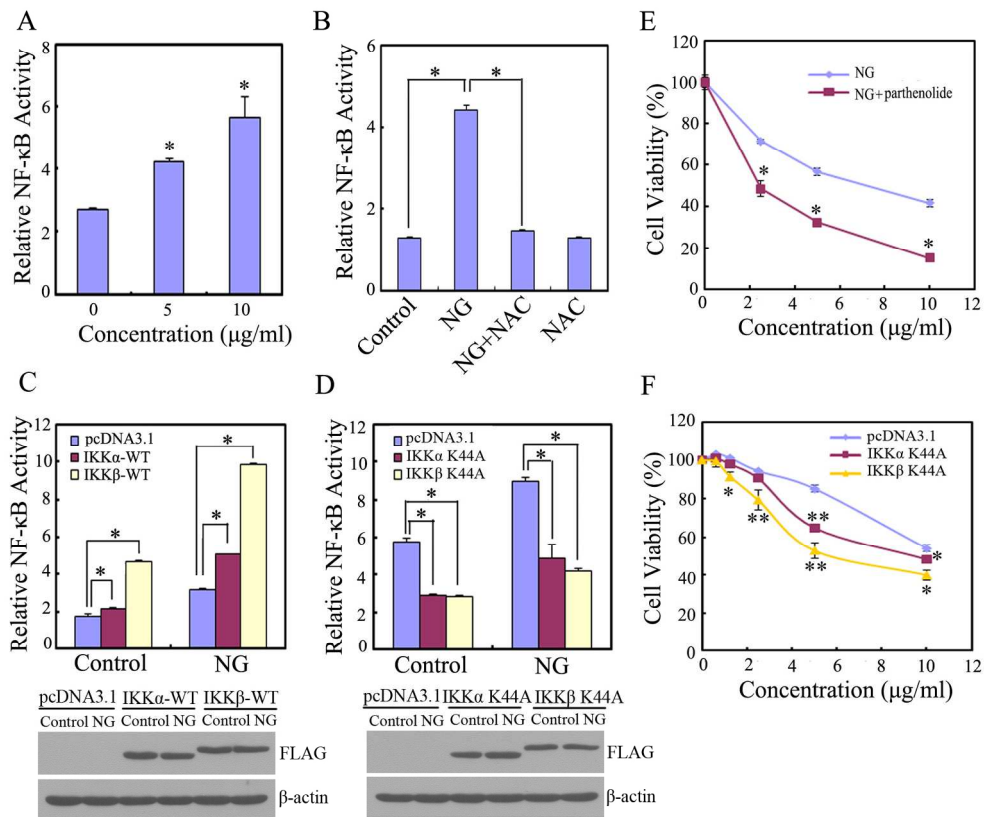
167x122mm (300 x 300 DPI)

Figure 6



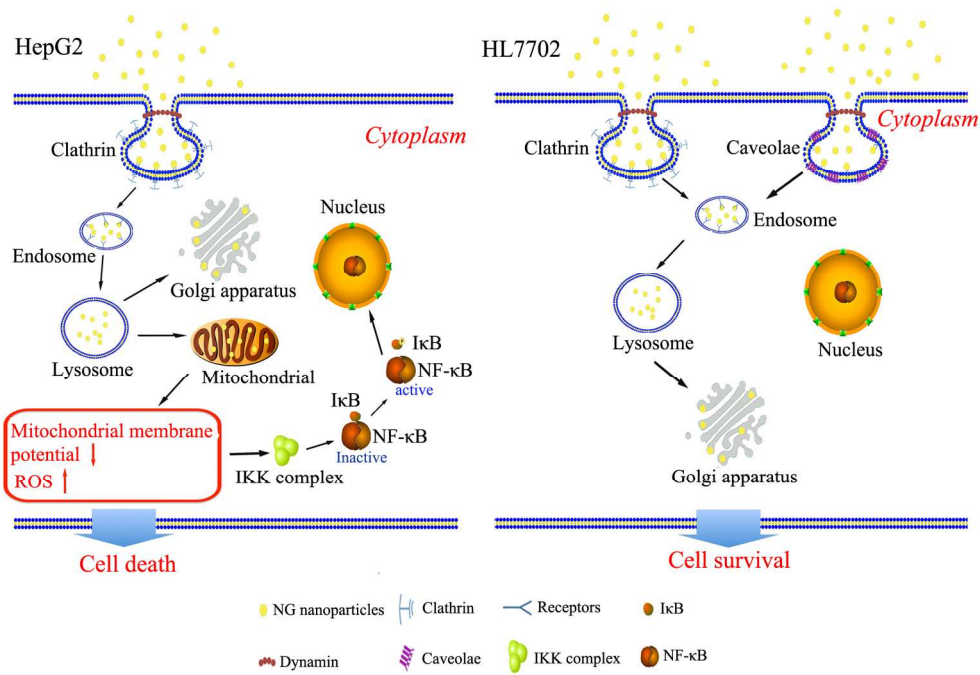
172x242mm (300 x 300 DPI)

Figure 7



177x156mm (300 x 300 DPI)

Figure 8



177x128mm (300 x 300 DPI)